Applied Catalysis B: Environmental 84 (2008) 341–350

Contents lists available at ScienceDirect

Applied Catalysis B: Environmental

journal homepage: www.elsevier.com/locate/apcatb

Low temperature NO_x and N_2O reduction by H_2: Mechanism and development of new nano-catalysts

Sounak Roy [a], M.S. Hegde [a], S. Sharma [a], N.P. Lalla [b], A. Marimuthu [c], Giridhar Madras [c,*]

[a] Solid State and Structural Chemistry Unit, Indian Institute of Science, Bangalore 560012, India
[b] UGC-DAE Consortium for Scientific Research, Khandwa Road, Indore 452017, India
[c] Chemical Engineering Department, Indian Institute of Science, Bangalore 560012, India

ARTICLE INFO

Article history:
Received 21 February 2008
Received in revised form 10 March 2008
Accepted 10 April 2008
Available online 18 April 2008

Keywords:
NO reduction by hydrogen
Metal ion-doped titanium oxide
Reaction mechanism

ABSTRACT

The understanding of the mechanistic aspects and development of new catalysts for NO_x reduction is a priority area of research. Precious metal substituted TiO_2 ($Ti_{0.99}M_{0.01}O_{2-\delta}$, where M = Ru, Rh, Pd, Pt) catalysts have been synthesized and investigated for the catalytic reduction of NO by H_2. These catalysts have higher activity compared to other catalysts reported in literature. The rate of NO reduction by H_2 depends on the reducibility of the catalysts. Temperature programmed reduction experiments with H_2 indicate that as the H_2 dissociation temperature decreases (reflecting the reducibility of the catalysts), the rate of NO + H_2 reaction increases. A new bi-functional reaction mechanism has been developed that accounts for NO adsorption on M^{n+} and NO dissociation on the oxide ion vacancy. The kinetic parameters were determined by fitting the model to the experimental data. Consistent with the experimental results, it was found that NO reduction rate was dependent on the adsorption and dissociation of H_2 on the metal.

1. Introduction

The emissions of NO_x from vehicular and stationary engines have significant environmental implications like acid rain, formation of ground level ozone (smog), stratospheric ozone depletion and associated health hazards [1]. Therefore, decomposition of NO_x has become a major challenge to the environmental scientists. NO is thermodynamically unstable ($NO \rightarrow 1/2N_2 + 1/2O_2$, $\Delta G_f^\circ = -86$ kJ/mol). However, the decomposition reaction has an activation energy of 364 kJ/mol and, therefore, a catalyst is necessary to lower the activation energy in order to facilitate this decomposition [2]. To reduce NO_x to N_2, various carbonaceous reductants like CO, hydrocarbons or non-carbonaceous reductants like H_2 and NH_3 are used. When CO or hydrocarbons are used, CO_2 (a green house gas) is produced. Non-carbonaceous NH_3, which is toxic, is widely used in selective catalytic reduction of NO_x. Also problems faced by the current NH_3-SCR technology [3], such as ammonia slip, ash odor, air-heaters fouling and high running cost, demand the finding of appropriate non-carbon-containing reducing agents. Thus H_2 can be used as a reductant, which is also present in the emission of the automobile and stationary sources [4–11].

The reaction of NO with H_2 can occur by the following steps:

$$2NO + 2H_2 \rightarrow N_2 + 2H_2O \quad (A)$$

$$2NO + H_2 \rightarrow N_2O + H_2O \quad (B)$$

$$2NO + 5H_2 \rightarrow 2NH_3 + 2H_2O \quad (C)$$

In the reactions (B) and (C), undesirable products N_2O and NH_3 are formed. It has been concluded that N_2 forms by dissociative chemisorption of NO, whereas N_2O forms from molecularly adsorbed NO species [11] in case of certain catalysts, as observed in our previous studies [12]. Therefore, new catalysts that can increase the dissociative chemisorption of NO are needed to achieve the more selective NO reduction by H_2 to N_2 (reaction (A)). The other important factor of this reaction is H_2 dissociation. Tauster et al. [13] showed the effect of strong metal support interaction (SMSI) on noble metal supported reducible oxides. The charge transfer from the reduced surface cations in SMSI state to the supported metal reduces the adsorption property of the catalyst. Therefore, a catalyst that has a reduced adsorption capacity in its SMSI state cannot be a good catalyst for NO reduction by H_2. Therefore, a catalyst needs to be developed such that it would dissociate H_2 at low temperatures and not reach the SMSI state. The other important aspect of this reaction is to

* Corresponding author. Tel.: +91 80 2293 2321; fax: +91 80 2360 0683.
E-mail addresses: giridhar@chemeng.iisc.ernet.in, giridharmadras@gmail.com (G. Madras).

0926-3373/$ – see front matter © 2008 Elsevier B.V. All rights reserved.
doi:10.1016/j.apcatb.2008.04.008

dissociate the intermediate N_2O, which is formed in the reaction (B) and thus increase the product selectivity of nitrogen.

The NO reduction by H_2 over oxidized and reduced Rh supported catalysts has been investigated but selectivity of N_2 to N_2O was low [5]. A small enhancement of selectivity was observed when Rh was used with Sn [6]. No significant change was observed in the reaction rate and the product selectivity with other Group VIII metals. Pt was used as a catalyst for the reaction, but the formation of ammonia was significant at high concentrations of H_2 [6]. However, latter some other studies showed that the formation of NH_3 and N_2O can be lowered by changing the support from SiO_2 or CeO_2 to $La_{0.7}Sr_{0.2}Ce_{0.1}FeO_3$ or $La_{0.5}Ce_{0.5}MnO_3$ [14,15].

The objective of this study was to synthesize and investigate new catalysts for NO reduction by H_2. Pt^{2+} ion-doped CeO_2 showed high rates of $H_2 + O_2$ reaction indicating high rates of H_2 as well as O_2 dissociation [16]. Pt as well as Pd ion-doped TiO_2 also showed high rates of $H_2 + O_2$ reaction. Rh and Ru ions in CeO_2 as well as in TiO_2 showed lower temperature reduction by hydrogen indicating hydrogen dissociation. H_2 adsorbed on $Ce_{0.98}Pt_{0.02}O_{2-\delta}$ is shown to be the precursors for dissociation in terms of longer H–H bond. NMR study showed the protonic hydrogen ($H^{\delta+}$ in nature) over the catalysts [17]. In lean-burn engines and in diesel engines, excess amount of oxygen is present (~5 vol%). Selectively reducing NO in presence of excess O_2 is more challenging because H_2 can be easily consumed by reacting with O_2 to form water [18–20]. In this work, however, we first attempt to develop a catalyst with high N_2 selectivity and higher rate in absence of oxygen and our future work will investigate the reaction in detail. All these noble metal ions are also known to adsorb NO. Therefore, ionically substituted precious metals in TiO_2 ($Ti_{0.99}M_{0.01}O_{2-\delta}$, M = Ru, Rh, Pd, Pt) were considered as right materials for NO reduction by H_2. The H_2-uptake study was carried out over the catalysts and a strong correlation was found with H_2 dissociation and NO + H_2 reaction over the catalysts. The intermediate reaction of N_2O reduction by H_2 was also investigated. A mechanistic model was developed to determine the kinetics.

2. Experimental

2.1. Synthesis of catalysts

One atmosphere percentage M/TiO_2 (M = Ru, Rh, Pd, Pt) have been prepared by single step solution combustion method. The combustion mixture for the preparation of M/TiO_2 catalyst contained stoichiometric amount of titanyl nitrate ($TiO(NO_3)_2$), precious metal salts ($RuCl_3$ (E. Marck India Ltd., 99.9%), $RhCl_3{\cdot}xH_2O$ (Arora Matthey Ltd., 40% Rh), $PdCl_2$ (S.D. Fine-Chem. Ltd., 99.9%), H_2PtCl_6 (Ranbaxy Laboratories Ltd., 99.9%)) and glycine (CH_2NH_2COOH). In brief, $TiO(NO_3)_2$ and the precious metal salts have been taken in the molar ratio of 0.99:0.01, with a calculated amount of the fuel (glycine). This was made into a homogeneous solution and introduced into a muffle furnace maintained at 350 °C. The solution after burning produced a voluminous solid product. A detailed discussion of the synthesis is provided in our previous work [21].

2.2. Characterization of catalysts

Catalysts were characterized by powder X-ray diffraction (XRD) and X-ray photoelectron spectroscopy (XPS). XRD patterns of oxide samples were recorded on a Phillips X'Pert diffractometer using Cu Kα radiation at a scan rate of $2\theta = 0.5^\circ$/min. XPS of the as prepared catalysts and used catalysts were recorded on an ESCA-3 Mark II VG scientific spectrometer using Al Kα radiation (1486.6 eV). Binding energies of core levels of metal ions are with reference to C (1s) at 285 eV and accurate within ± 0.2 eV. For XPS analysis the as-prepared catalyst samples were made into pellets of 8 mm diameter and placed in a ultrahigh vacuum (UHV) chamber at 10^{-9} Torr housing the analyzer. High-resolution transmission microscopy (HRTEM) was carried out using a JEOL JEM-200-CX transmission electron microscope.

In a H_2-temperature programmed reduction (H_2-TPR) run of the catalyst sample of 40–80 mesh size was plugged with ceramic wool in a continuous flow reactor of length 30 and 0.4 cm internal diameter with the H_2 flow at a linear heating rate of 10 °C min^{-1}. There was no pressure drop across the reactor. Wherever required, the low temperature was achieved by liquid nitrogen flush for few minutes. The amount of H_2-uptake was detected by a thermal conductivity detector (TCD), which was calibrated against the uptake of H_2 with a known amount of CuO.

Electrochemical measurements were carried out using potentiostate–galvanostate (Techno Sci. Instruments, Bangalore). Electrodes were made by mixing equal amount of catalysts with carbon powder and coating the same on a graphite sheet on 1 cm^2 area. Polyvinyledene difluoride (PVDF) was used as a binder and *N*-methylpyrrolidone as a solvent. Electrical contacts were made using stainless steel sheet and silver paste. Cyclic voltametric experiments were performed at a constant scan rate of 40 mV s^{-1} in the potential range of −0.1–1.2 V. Chronopotentiometric experiments were performed for 5000 s keeping a constant current of −0.1 mA.

2.3. Catalytic tests

The catalytic reactions were carried out in a temperature programmed reaction system equipped with a quadrupole mass spectrometer SX200 (VG Scientific Ltd., England) and a gas chromatograph (GC) (Mayura Analytical, India). The catalyst samples were packed between two glass wool plugs in the center of a quartz tube of 4 mm internal diameter, inserted into a furnace heated to the required reaction temperature through a temperature controller. The reaction temperature was measured by chromel–alumel thermocouple dipped in the catalyst bed. The gaseous products were sampled from the output stream through a fine leak valve via differential pumped sampling chamber to an ultra-high-vacuum (UHV) system housing the quadrupole mass spectrometer. An online GC equipped with Hayesep Q column analyzed the products through TCD detector. The oven was kept constant at 100 °C, injector and the detector was at 50 °C. Typically 40–80 mesh of catalyst was used with SiO_2 to make up the catalyst bed volume of 0.138 cm^3. The total flow rate was 100 cm^3 min^{-1} with gas hourly space velocity (GHSV) = 43,000 h^{-1}. Reactions were carried out with the ratio (vol%) of NO to H_2 maintained at 1:3. Gases are from M/S Bhuruka Gases Ltd. (India) with 4.74 vol% NO in He, 5.21 vol% N_2O in H_2, 10.49 vol% H_2 in He and 5.14% CO in He.

3. Results and discussion

3.1. Structural studies

XRD patterns of $1\%M/TiO_2$ (M = Ru, Rh, Pd, Pt) are shown in Fig. 1. The diffraction lines of $1\%M/TiO_2$ (M = Ru, Rh, Pd, Pt) are indexed to anatase structure. A rutile contribution was observed to the extent of 10% only for $1\%Ru/TiO_2$. No diffraction lines due to the precious metals or precious metal oxides were observed in $1\%M/TiO_2$(M = Ru, Rh, Pd, Pt). Rietveld refinements of the four catalysts were done taking the substituted noble metals in Ti^{4+} (4a) position and plotted in Fig S1–4. The cell parameters are given in Table 1. A slight increase in cell volume is observed for $1\%Pt/TiO_2$ due to

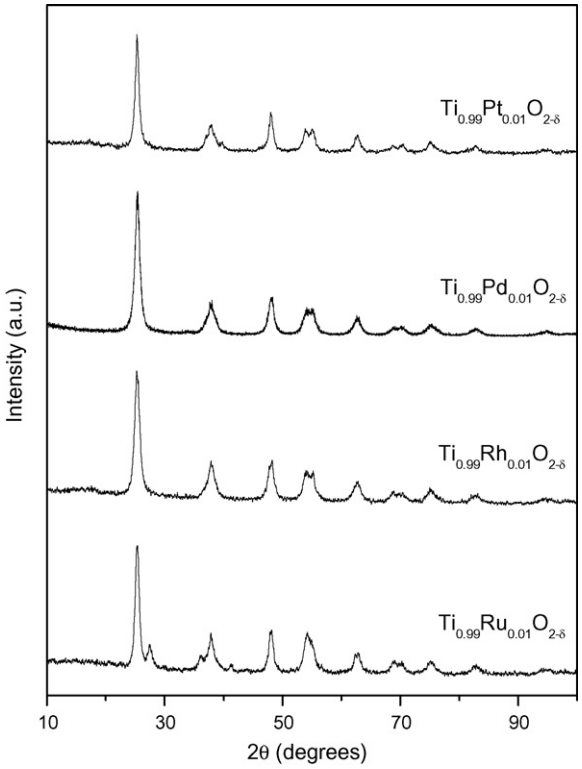

Fig. 1. XRD pattern of $Ti_{0.99}M_{0.01}O_{2-\delta}$.

slight increase in ionic radius of Pt, however, there is almost no change in cell volume as well as cell parameters for Rh, Ru and Pd ion-doped TiO_2. The particle sizes measured from Scherrer's formula are in the range of 10–15 nm for the four catalysts.

HRTEM image of 1%Pd/TiO_2 is given in Fig. 2a and no Pd or PdO particles were observed. The fringes in HRTEM micrographs, i.e. (1 0 1) plane of TiO_2 correspond to 3.5 Å. The particle sizes measured from the image are in the range of 10–12 nm, which agrees well with the size determined from XRD. Fig. 2b shows the electron diffraction pattern of 1%Pd/TiO_2. The ring-type diffraction pattern is indexed to polycrystalline TiO_2 in anatase structure and no line corresponding to Pd or PdO was detected.

In Fig. 3, core-level XPS of (a) Ru (3p) of 1%Ru/TiO_2, (b) Pd (3d) of 1%Pd/TiO_2, (c) Pt (4f) of 1%Pd/TiO_2 and (d) Rh (3d) of 1%Pd/TiO_2 are presented. The highest intense XP spectrum of Ru is the 3d region. The Ru ($3d_{3/2}$) peak is entirely overlapped by the high intense C (1s) peak. Further, the Ru ($3d_{5/2}$) is also partially covered by the C (1s) peak. Therefore, it is difficult to analyze this region. So, Ru (3p) spectra is plotted in Fig. 3a, and from the Ru ($3p_{3/2}$) at 463 eV, it is clear that Ru is in 4^+ state similar in RuO_2. The Pd ($3d_{5/2}$) peak at 337.2 eV indicates Pd^{2+} ion substitution in TiO_2. Further studies showed that Pd^{2+} ions in TiO_2 is more ionic than Pd^{2+} in PdO with Pd^{2+}($3d_{5/2,3/2}$) peaks at 336.8 and 342.2 eV [21]. Pt (4f) of $Ti_{0.99}Pt_{0.01}O_{2-\delta}$ showed a broad spectrum of mixed

Table 1
Rietveld refinement parameters of TiO_2 and $Ti_{0.99}M_{0.01}O_{2-\delta}$ (M = Ru, Rh, Pd, Pt)

Catalysts	a/b (Å)	c (Å)	R_{BRAGG}	χ^2
TiO_2	3.790 (4)	9.506 (7)	2.64	1.50
$Ti_{0.99}Ru_{0.01}O_{2-\delta}$	3.785 (3)	9.490 (4)	11.40	1.88
$Ti_{0.99}Rh_{0.01}O_{2-\delta}$	3.789 (7)	9.490 (4)	6.08	1.15
$Ti_{0.99}Pd_{0.01}O_{2-\delta}$	3.786 (5)	9.510 (2)	2.65	1.01
$Ti_{0.99}Pt_{0.01}O_{2-\delta}$	3.790 (2)	9.524 (1)	6.79	1.28

The number in brackets refers to the inaccuracies in that digit.

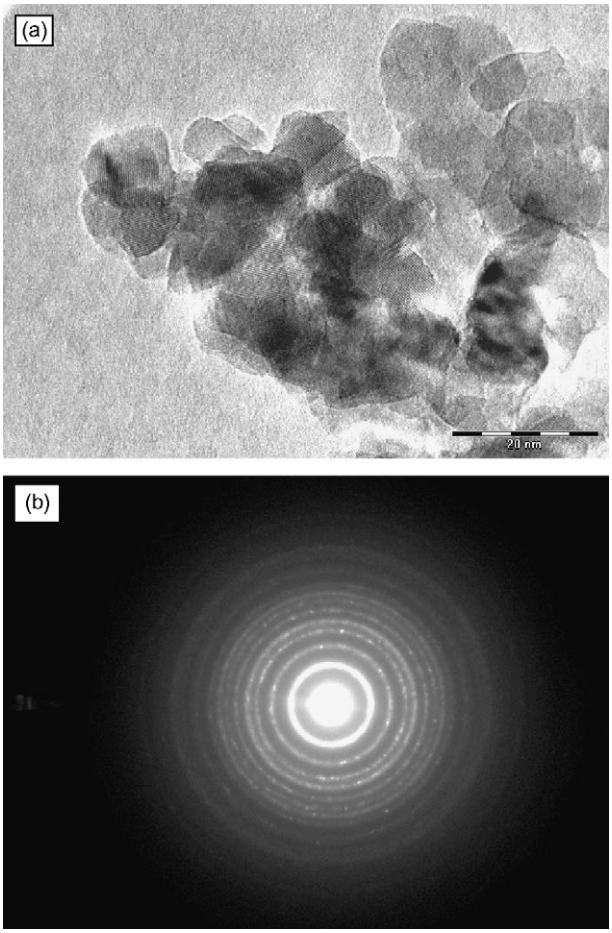

Fig. 2. (a) HRTEM image of $Ti_{0.99}Pd_{0.01}O_{2-\delta}$ and (b) is the ED pattern of the same.

valence state of Pt^{2+} and Pt^{4+}. When deconvoluted $4f_{7/2}$ at 72.0 eV indicates Pt^{2+}, whereas $4f_{7/2}$ at 75.4 eV indicates Pt^{4+} state, and the peak intensity ratio of Pt^{2+} to Pt^{4+} is 1.5 [22]. Rh ($3d_{5/2}$) at 310.0 eV indicates clearly Rh is in 3^+ state [23]. Thus, Pd ion is indeed substituted in TiO_2 crystallites. Surface concentration of M^{n+} $Ti_{0.99}M_{0.01}O_{2-\delta}$ and metal dispersed over TiO_2 is estimated from the relative intensities of M (3d/4f/3p) and Ti ($2p_{3/2,1/2}$) core level spectra [24]:

$$\frac{X_{Pd}}{X_{Ti}} = \frac{I_M}{I_{Ti}} \frac{\sigma_{Ti}\lambda_{Ti}D_E(Ti)}{\sigma_M\lambda_M D_E(M)}$$

where X, I,σ, λ and D_E are the surface concentration, intensity, photoionization cross section, mean escape depth, and geometric factors, respectively. Mean escape depth values and photoionization cross sections were obtained from literature [24,25]. Accordingly, surface concentration of Pd^{2+} ion in $Ti_{0.99}Pd_{0.01}O_{2-\delta}$ is 2.3%, Rh^{3+} ion in $Ti_{0.99}Rh_{0.01}O_{2-\delta}$ is 4.4%, Ru^{4+} ion in $Ti_{0.99}Ru_{0.01}O_{2-\delta}$ is 5.13% and Pt^{2+} in $Ti_{0.99}M_{0.01}O_{2-\delta}$ is 4.79%. Thus, all the noble metals are segregated on the surface of TiO_2. Since there are no metal particles, ions are substituted in the lattice. Since the catalysts are heated during the preparation, surface segregation is observed. Because the noble metals are in ionic form, oxide ion vacancies are created for charge balance. The catalysts are represented by $Ti_{0.99}M_{0.01}O_{2-\delta}$, where M = Ru, Rh, Pd, Pt.

3.2. Hydrogen uptake studies

H_2-uptake experiments were carried out over $Ti_{0.99}M_{0.01}O_{2-\delta}$ (M = Ru, Rh, Pd, Pt) from −50 to 500 °C. Fig. 4 shows H_2-TPR profiles

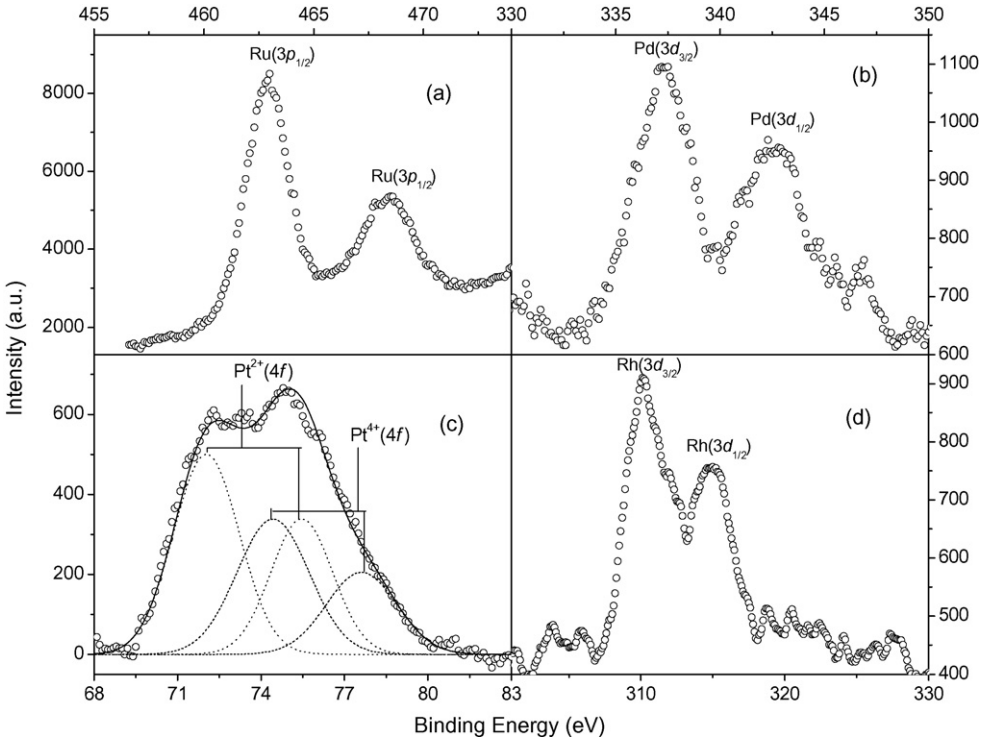

Fig. 3. Core-level XPS of (a) Ru (3p) of $Ti_{0.99}Ru_{0.01}O_{2-\delta}$, (b) Pd (3d) of $Ti_{0.99}Pd_{0.01}O_{2-\delta}$, (c) Pt (4f) of $Ti_{0.99}Pt_{0.01}O_{2-\delta}$ and (d) Rh (3d) of $Ti_{0.99}Rh_{0.01}O_{2-\delta}$.

for all the catalysts and the precious metal oxides M_xO_y. There are distinct differences between the precious metal oxides and the substituted TiO_2 catalysts. In general for all the substituted TiO_2 catalysts, there is one sharp peak at low temperature and a broad peak at higher temperature region. Unsubstituted TiO_2 shows very little H_2-uptake and the reduction starts above 375 °C (Fig. S5). So, the higher temperature broad peak for the substituted catalysts can be attributed to the reduction of TiO_2. For $Ti_{0.99}Ru_{0.01}O_{2-\delta}$ shows the first peak at 175 °C, while RuO_2 shows a peak at 135 °C. $Ti_{0.99}Rh_{0.01}O_{2-\delta}$ shows the first peak at 32 °C, while Rh_2O_3 shows a peak at 182 °C. For $Ti_{0.99}Pd_{0.01}O_{2-\delta}$ the first peak is at −5 °C and for $Ti_{0.99}Pt_{0.01}O_{2-\delta}$, there are three low temperature peaks designated as α (highest intense peak), β and γ at −3, 34 and 90 °C, respectively. So, among all the catalysts $Ti_{0.99}Ru_{0.01}O_{1.99}$ showed the highest temperature reduction peak, followed by $Ti_{0.99}Rh_{0.01}O_{1.99}$, whereas $Ti_{0.99}Pd_{0.01}O_{1.99}$ and $Ti_{0.99}Pt_{0.01}O_{1.99}$ showed the lowest temperature reduction peak. Therefore the first low temperature peak can be attributed to the reduction of M^{n+} ions in TiO_2. As for all the precious metal oxides, M_xO_y (except RuO_2 and $Ti_{0.99}Ru_{0.01}O_{2-\delta}$) show the reduction peak at higher temperature than the substituted TiO_2 ($Ti_{0.99}M_{0.01}O_{2-\delta}$) catalysts, there must be metal–support interaction which reduces the precious metal reduction temperature. To verify this, experiments were conducted using the same metal (Pd) on different supports. For example, $Ti_{0.99}Pd_{0.01}O_{2-\delta}$ and 1%Pd/Al_2O_3 shows the Pd^{2+} reduction peak at different temperature (Fig. S5). The catalysts were re-oxidized in O_2 at 500 °C and in the second cycle, H_2-TPR also shows the similar signal indicating H_2-uptake is reversible. H_2/M molar ratio taking only the first peak the case of $Ti_{0.99}Ru_{0.01}O_{2-\delta}$, $Ti_{0.99}Rh_{0.01}O_{2-\delta}$, $Ti_{0.99}Pd_{0.01}O_{2-\delta}$ and $Ti_{0.99}Pt_{0.01}O_{2-\delta}$ is 1.02, 2.09, 1.9 and 4.4, respectively. The molar H_2/Pd ratio with PdO sample is close to unity with the chemical reaction $H_2 + PdO \rightarrow Pd^{\circ} + H_2O$, and the negative peak at ~40 °C is attributed with PdH_x. H_2 from PdH_x can release with the rise in temperature and the negative peak occurs. The area under the negative peak corresponds to $x = 6$. Low temperature H_2 adsorption on $Ti_{0.99}Pd_{0.01}O_{1.99}$ does not evolve H_2O. H_2O is formed only upon passing O_2 at room temperature and H_2 can be again adsorbed quantitatively. Thus, the adsorbed H_2 can easily react with O_2 at room temperature to give H_2O indicating that H_2 on $Ti_{0.99}Pd_{0.01}O_{2-\delta}$ is either present in dissociated state or as a precursor to dissociation.

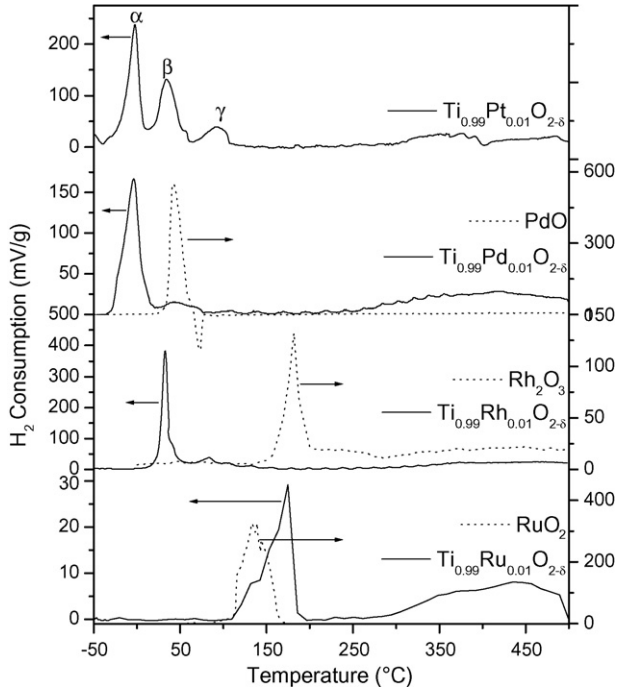

Fig. 4. H_2-TPR profile of $Ti_{0.99}M_{0.01}O_{2-\delta}$ and M_xO_y.

3.3. Electrochemical studies

Cyclic voltamogram (CV) of $Ti_{0.99}M_{0.01}O_{2-\delta}$ (M = Ru, Rh, Pd, Pt) in 0.5 M H_2SO_4 are given in Fig. 5. $Ti_{0.99}Pd_{0.01}O_{2-\delta}$ showed two peaks at 0.46 and 0.41 V for dissolved O_2 oxidation and reduction, respectively. These peaks indicate the redox activity of $Ti_{0.99}Pd_{0.01}O_{2-\delta}$ is high. In deaereted electrolyte these peaks vanish. Polarization in anode side starting above 1.1 and at ~0 V in the cathode side is also observed. The redox behavior becomes constant after 5th cycle (not shown). For comparison 2nd, 20th and 40th cycles are plotted. Constant response in CV in 20th and 40th cycle is apparent. CV of $Ti_{0.99}Pt_{0.01}O_{2-\delta}$ dissolved O_2 oxidation and reduction peaks are less prominent compared to $Ti_{0.99}Pd_{0.01}O_{2-\delta}$, which must show comparatively lesser redox activity. The CV response also indicates a resistance in the $Ti_{0.99}Pt_{0.01}O_{2-\delta}$ matrix, as the voltamogram is shifted. Also, the subsequent cycles did not

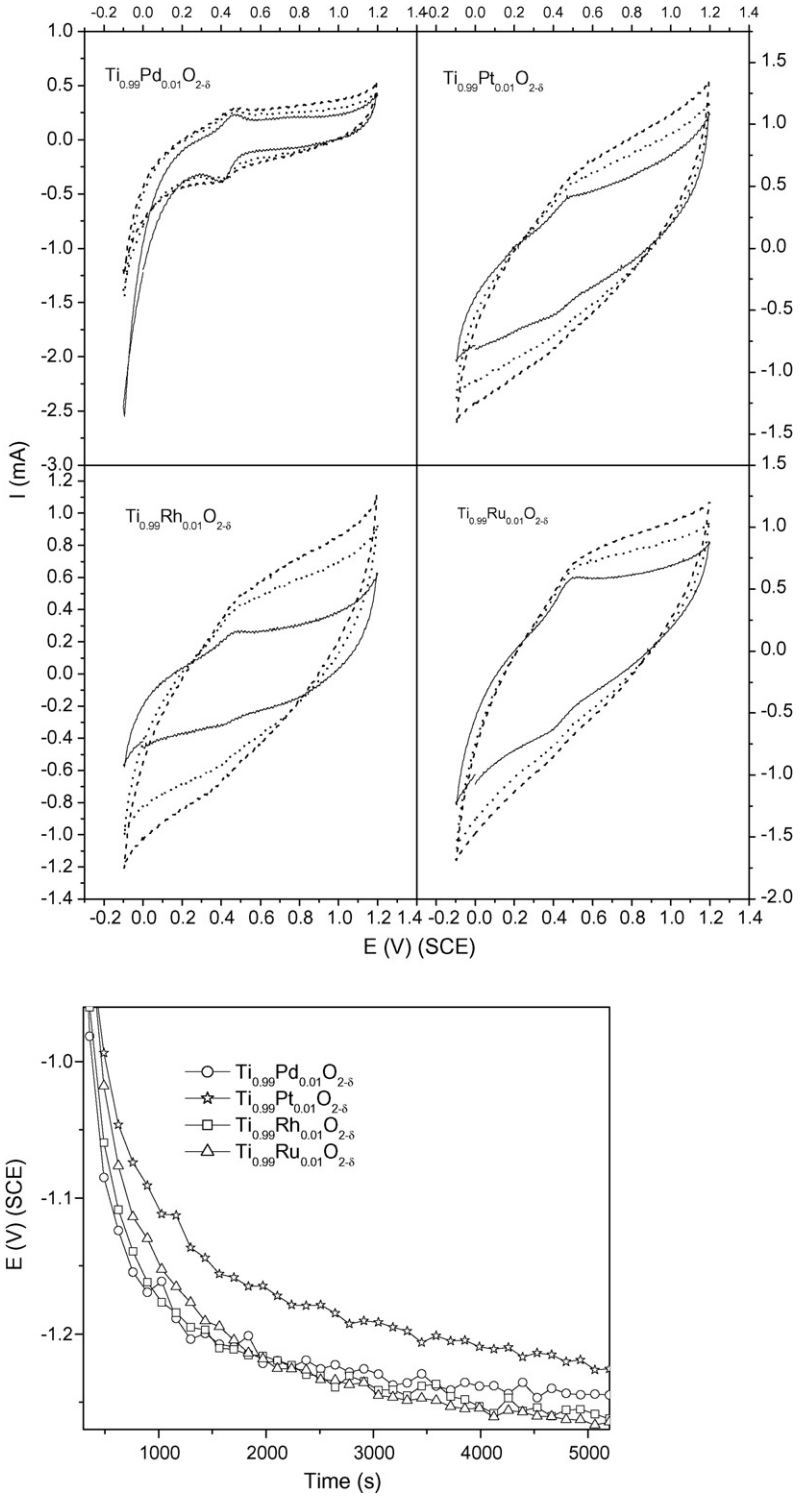

Fig. 5. (a) CV of $Ti_{0.99}M_{0.01}O_{2-\delta}$. Solid line indicates the 2nd cycle whereas the dotted and the dashed lines indicate 20th and 40th cycle, respectively. (b) Chronopotentiometric curve of $Ti_{0.99}M_{0.01}O_{2-\delta}$.

give a constant response and resistance seems to be increasing. The similar explanation holds true for $Ti_{0.99}Rh_{0.01}O_{2-\delta}$ also. The only difference between $Ti_{0.99}Pt_{0.01}O_{2-\delta}$ and $Ti_{0.99}Rh_{0.01}O_{2-\delta}$ is the resistance in the later one increase more from 2nd to 20th to 40th scan, which will hamper its redox activity further. In $Ti_{0.99}Ru_{0.01}O_{2-\delta}$, a capacitance behavior (square wave) was observed indicating the presence of RuO_2 in $Ti_{0.99}Ru_{0.01}O_{2-\delta}$. Due to this behavior its redox activity should be inferior to the other catalysts as confirmed from H_2-Uptake studies and will be proved in following catalytic studies. Further confirmation of the redox activity was done by performing chronopotentiometric experiments (Fig. 5b) where we have monitored the potential gain with respect to time at constant current. We find that potential required drawing 0.001 mA current is least for $Ti_{0.99}Pd_{0.01}O_{2-\delta}$ followed by $Ti_{0.99}Pt_{0.01}O_{2-\delta}$ $Ti_{0.99}Rh_{0.01}O_{2-\delta}$ and $Ti_{0.99}Ru_{0.01}O_{2-\delta}$ with the potential values of 1.23, 1.24, 1.26 and 1.27 V. Thus the redox catalytic activity must follow the same order and indeed activity was found to be in the same order.

Surface area measurements showed that $Ti_{0.99}Pt_{0.01}O_{2-\delta}$ has surface area 27.0 $m^2\ g^{-1}$, whereas $Ti_{0.99}Pd_{0.01}O_{2-\delta}$, $Ti_{0.99}Rh_{0.01}O_{2-\delta}$ and $Ti_{0.99}Ru_{0.01}O_{2-\delta}$ have surface area 50.0, 52.3 and 55.7 $m^2\ g^{-1}$, respectively.

3.4. Catalytic studies

3.4.1. NO reduction by H_2

NO reduction by H_2 was carried out over the catalysts $Ti_{0.99}M_{0.01}O_{2-\delta}$ at a steady state condition. The ratio of the weight of the catalyst, W, to the flow rate of NO, F_{NO}, was kept constant at 201.5×10^3 g mol^{-1}. The products detected were N_2, N_2O, NH_3 and H_2O. Light off curve in Fig. 6 shows the NO conversion over $Ti_{0.99}M_{0.01}O_{2-\delta}$ (M = Ru, Rh, Pd, Pt). T_{50} (temperature at 50% conversion) of NO conversion over the catalysts $Ti_{0.99}Ru_{0.01}O_{2-\delta}$, $Ti_{0.99}Rh_{0.01}O_{2-\delta}$, $Ti_{0.99}Pd_{0.01}O_{2-\delta}$ and $Ti_{0.99}Pt_{0.01}O_{2-\delta}$ are at 281, 140, 88 and 83 °C. Except for $Ti_{0.99}Pt_{0.01}O_{2-\delta}$, NO conversion increases monotonically with temperature, whereas the conversion shows a step in presence of $Ti_{0.99}Pt_{0.01}O_{2-\delta}$. It is very interesting to observe that there is a strong correlation with the H_2 adsorption temperature in H_2-TPR experiment and the NO conversion temperature. Higher the H_2 adsorption temperature, higher is the T_{50} of NO reduction. This indicates that the catalyst that adsorbs H_2 easily at low temperature will be a better catalyst for NO reduction by H_2. This provides an input to the mechanism of the reaction. NO reduction to N_2 occurs via the NO dissociation step. So, if the rate of NO reduction and NO conversion to N_2 is high, there has to be more NO dissociation, which takes place in the oxide ion vacancy site of the catalysts. The precious metals, which adsorb H_2 easily below room temperature, will direct NO to dissociatively chemisorb in the oxide ion vacancy site. The NO reduction occurs at low temperature in presence of $Ti_{0.99}Pt_{0.01}O_{2-\delta}$ and $Ti_{0.99}Pd_{0.01}O_{2-\delta}$. Whereas, NO reduction takes place at comparatively at higher temperature for $Ti_{0.99}Rh_{0.01}O_{2-\delta}$ and $Ti_{0.99}Ru_{0.01}O_{2-\delta}$. To prove this point further, we checked out the CO poisoning effect over the catalysts. Among all the four precious metals, Pt has the most CO adsorption propensity [13]. In the feed gas flow, 1 vol% CO in He was fed with NO and H_2. Fig. 7 shows the NO reduction by H_2 profile over the four catalysts in presence of CO (at this temperature range NO reduction by CO does not take place over these catalysts [18], it is only NO reduction by H_2). NO reduction by H_2 does not take place completely over $Ti_{0.99}Pt_{0.01}O_{2-\delta}$ and $Ti_{0.99}Rh_{0.01}O_{2-\delta}$, where CO adsorption propensity is high and H_2 dissociation cannot take place due to CO covered surface [26], whereas for $Ti_{0.99}Pd_{0.01}O_{2-\delta}$ and $Ti_{0.99}Ru_{0.01}O_{2-\delta}$, where CO adsorption is low, there is a little change in the NO conversion profile. This again proves the importance of H_2 adsorption/dissociation for this reaction. However, it was observed that the surface area of the catalysts does not play any role in the NO + H_2 reaction.

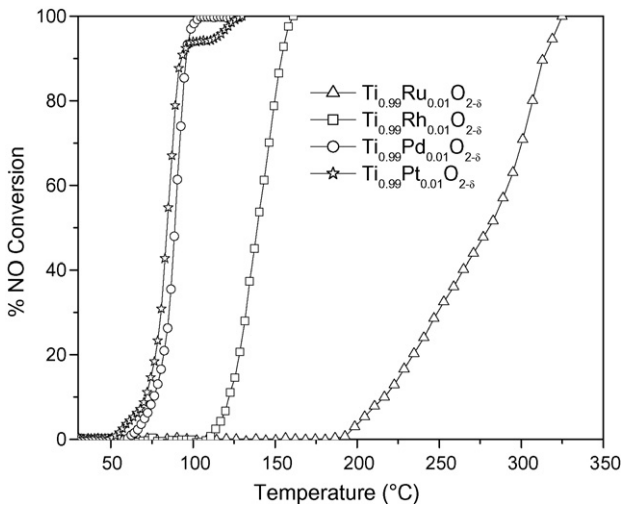

Fig. 6. Light off curve of NO reduction by H_2 over $Ti_{0.99}M_{0.01}O_{2-\delta}$.

The N_2, N_2O and NH_3 selectivity over all the catalysts during NO reduction by H_2 is plotted in Fig. 8. $Ti_{0.99}Pd_{0.01}O_{2-\delta}$ shows the lowest N_2O formation among the four catalysts. Among all the four catalysts, $Ti_{0.99}Rh_{0.01}O_{2-\delta}$ shows the highest N_2O formation followed by $Ti_{0.99}Ru_{0.01}O_{2-\delta}$. The N_2O reduction to N_2 needs N_2O dissociation as an elementary step. It is apparent from the above discussion that over $Ti_{0.99}Pd_{0.01}O_{2-\delta}$, N_2O dissociates faster compared to other catalysts. We have done isolated N_2O reduction by H_2 over the catalysts, as discussed in the following section. NH_3, the other unselective product of the reaction, is also formed over the catalysts, except over $Ti_{0.99}Pd_{0.01}O_{2-\delta}$. The NH_3 selectivity of each catalyst is also shown in Fig. 8. Whereas $Ti_{0.99}Pd_{0.01}O_{2-\delta}$ does not show any NH_3 formation, $Ti_{0.99}Pt_{0.01}O_{2-\delta}$ shows the highest formation of NH_3. The absence of NH_3 formation over Pd supported catalysts has been pointed out earlier [27–30]. On the other hand, Pt supported catalysts showing a large amount of ammonia formation also have been well known for NO + H_2 reaction [7].

A comparative study over the metal–support catalysts available in published literature shows that the rates and the turn over frequencies (TOF) of NO conversion in NO + H_2 reaction over $Ti_{0.99}M_{0.01}O_{2-\delta}$ is orders of magnitude higher than the reported values (Table 2; Arrhenius plots of NO + H_2 reaction over $Ti_{0.99}M_{0.01}O_{2-\delta}$ are shown in Fig. 9a). Over 0.1 wt% $Pt/La_{0.7}Sr_{0.2}Ce_{0.1}FeO_3$ the TOF is slightly higher than $Ti_{0.99}M_{0.01}O_{2-\delta}$, however, the temperature (100 °C, where TOF was calculated) is higher than our calculation temperature. Normally, the N_2 selectivity increases with temperature, as observed for reactions over Pt/SiO_2 [6] and $Pt/CoO_x/SiO_2$ [6] and Rh/SiO_2 [4]. The selectivity of nitrogen is only 50% over Pt and Rh/Pt single crystals [7]. However, Barrera et al. have shown that N_2 selectivity in NO + H_2 reaction never exceeds 60% in presence of $Pd/Al_2O_3/La_2O_3$. Further, this selectivity reduces to 30% at higher temperatures [32]. Dhainaut et al. showed that the higher temperature reduction decreases the rate of the reaction [33].

Many mechanisms are proposed in the literature [7,10,33–36] for NO reduction by hydrogen over noble metal supported on non-reducible oxides such as SiO_2/Al_2O_3. The kinetics that has been described by these studies was based on the mono-functional

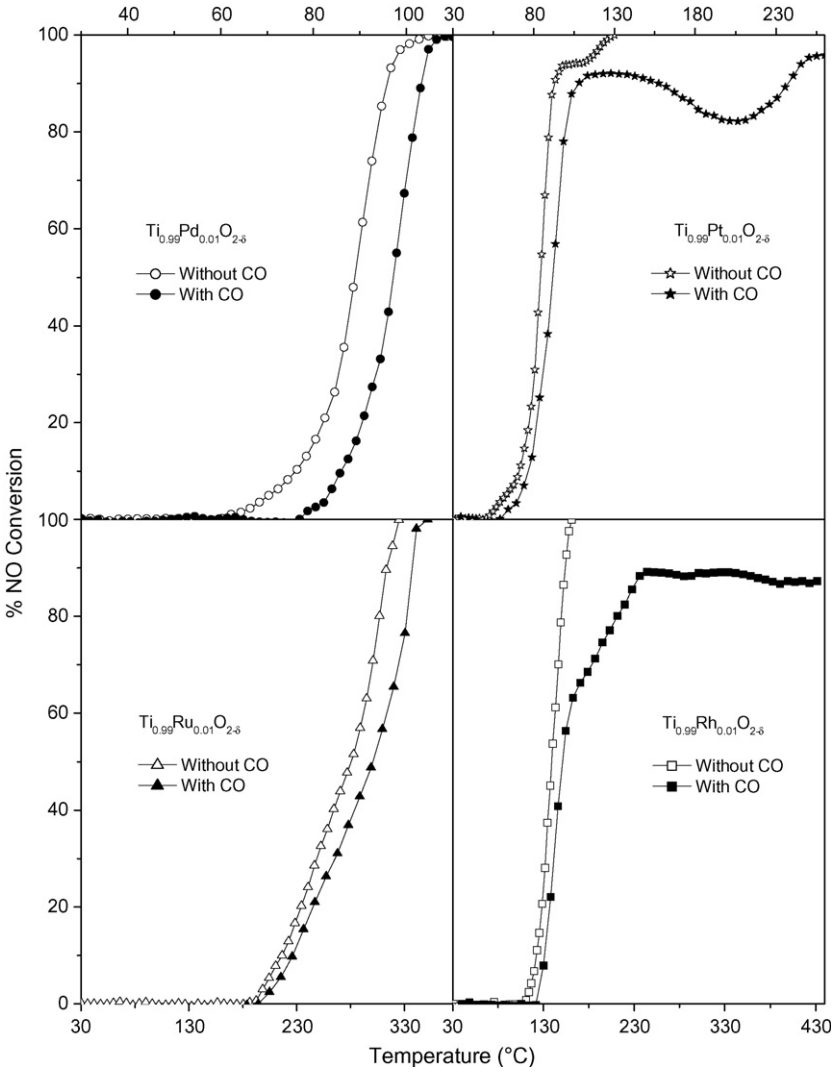

Fig. 7. CO tolerance effect over $Ti_{0.99}M_{0.01}O_{2-\delta}$.

Table 2
Parameters of NO + H_2 reaction over various reported catalysts

Catalysts	Rate (μmol g^{-1} s^{-1}) (°C)	TOF[a] (s^{-1}) (°C)	E_{NO} (kJ/mol)	Refs
$Pt/MNO_x/SiO_2$[b]	–	1.0×10^{-3} (50)	–	[6]
Pt/SiO_2[b]	–	3.1×10^{-4} (50)	–	–
$Pt/Rh/Al_2O_3$[b]	–	5.8×10^{-3} (75)	–	–
$Pt/La_{0.7}Sr_{0.2}Ce_{0.1}FeO_3$[c]	–	2.0×10^{-2} (100)	–	[15]
5% Pt/SiO_2[d]	1.5 (125)	–	–	[31]
Pd/Al_2O_3[e]	1.83 (70)	–	68.1	[33]
$Pd/LaCoO_3$ (Reduced at 450 °C)[f]	1.58 (110)	–	79.7	–
$Pd/LaCoO_3$ (Reduced at 250 °C)[g]	2.75 (110)	–	84.4	–
$Ti_{0.99}Pd_{0.01}O_{2-\delta}$	24.6 (70)	1.2×10^{-2} (70)	60.4	This work
$Ti_{0.99}Pt_{0.01}O_{2-\delta}$	43.3 (70)	1.2×10^{-2} (70)	42.2	
$Ti_{0.99}Rh_{0.01}O_{2-\delta}$	3.8 (110)	1.9×10^{-3} (110)	97.3	–
$Ti_{0.99}Ru_{0.01}O_{2-\delta}$	15 (200)	7.9×10^{-4} (200)	109.4	–

[a] TOF has been calculated for our work taking the total moles of Pd^{2+} ions present per gram of the catalyst, where for the other references it has been calculated by the total moles of surface transition metals present per gram of the catalyst.
[b] Total flow rate = 40 ml/min; NO:H_2 = 1:1.
[c] NO = 0.25 vol%, H_2 = 1 vol%.
[d] 1.8% of NO and H_2 with total flow of 103 ml/min.
[e] NO = 8.5×10^{-3} and H_2 = 8.8×10^{-3} atm.
[f] NO = H_2 = 8.9×10^{-3} atm.
[g] NO = 7.5×10^{-3} and H_2 = 8.4×10^{-3} atm.

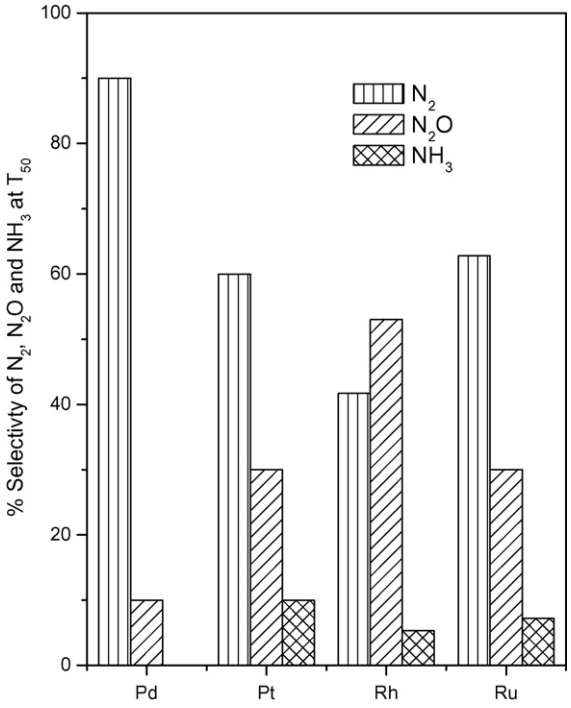

Fig. 8. Relative N_2O formation over $Ti_{0.99}M_{0.01}O_{2-\delta}$. NH_3 selectivity over the catalysts at T_{50} has been shown in inset.

mechanism in which the species are adsorbed only on the metal sites before yielding the products. Hoost et al. showed the evidence of metal–support interaction for the nitric oxide adsorption on Pd/Al_2O_3 [37]. Studies of NO reduction by H_2 in presence of Pd/Al_2O_3/TiO_2 have also been investigated. However, no mechanistic aspect has been described [27–29]. H_2-uptake studies clearly show its adsorption on M^{n+} site. According to previous studies [33,34] NO can be adsorbed both on M^{n+} site (molecular adsorption) as well as on the oxide ion vacant site (dissociative chemisorption). Based on the above considerations, the reaction mechanism over $Ti_{0.99}M_{0.01}O_{2-\delta}$ can be written as

$$H_2 + 2S_{Pd} \Leftrightarrow 2H_{Pd} \quad (1)$$

$$NO + S_{Pd} \Leftrightarrow NO_{Pd} \quad (2)$$

$$NO + \text{“V”} \Leftrightarrow \text{N“O”} \quad (3)$$

$$NO_{Pd} + \text{N“O”} \rightarrow N_2O + \text{“O”} + S_{Pd} \quad (4)$$

$$H_{Pd} + \text{“O”} \rightarrow \text{“O”H} + S_{Pd} \quad (5)$$

$$\text{“O”H} + H_{Pd} \rightarrow H_2O + \text{“V”} + S_{Pd} \quad (6)$$

$$N_2O + \text{“V”} \rightarrow N_2 + \text{“O”} \quad (7)$$

$$3H_{Pd} + \text{N“O”} \rightarrow NH_3 + \text{“O”} + S_{Pd} \quad (8)$$

Here “V” is the oxide ion vacancy on the support and S_M is the active site on M^{n+}. In the above mechanism, it is assumed that both NO and H_2 are in equilibrium on M^{n+} site and NO is also adsorbed on the oxide ion vacancy. The formation of N_2O (step (4)) occurs because of close proximity of nitrogen atom of NO_M and the nitrogen atom of N“O” adsorbed on vacancy site through oxygen. The hydrogen atom from the M^{n+} site reacts with the oxygen in oxide ion vacant site to form water in two steps (step (5) and (6)). N_2O gas molecule dissociates directly into N_2 and “O” due to the oxide ion vacancy (step (7)). Step (8) is not an elementary step in the mechanism but a combination of three steps, as discussed in detail in the derivation shown in S6 (see Appendix B Supporting information Fig. S6).

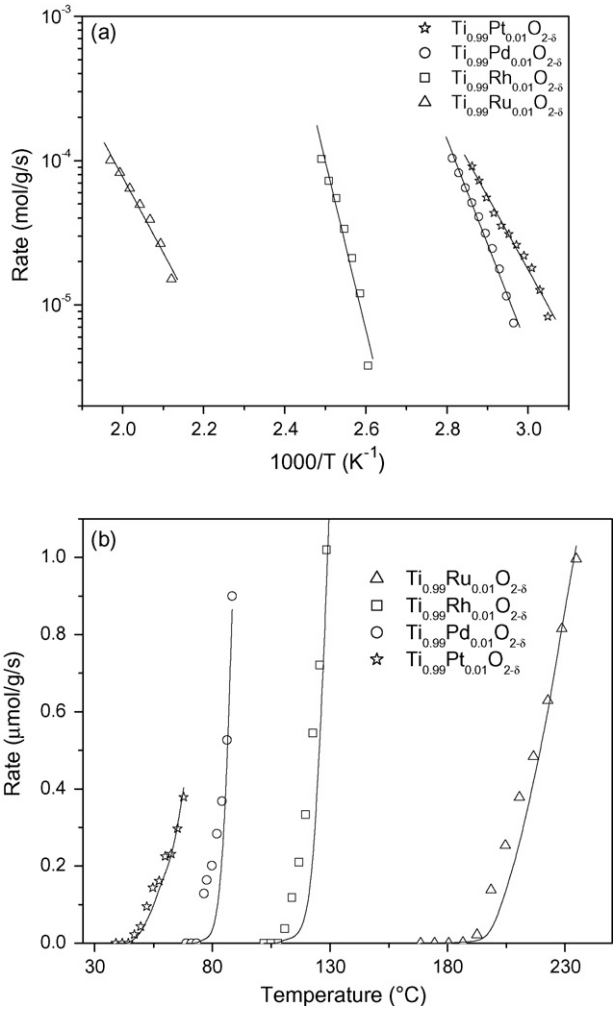

Fig. 9. (a) Arrhenius plot for the NO + H_2 over $Ti_{0.99}M_{0.01}O_{2-\delta}$ reaction to determine the activation energy. (b) Variation of reaction rate of NO + H_2 with temperature with the model fit over $Ti_{0.99}M_{0.01}O_{2-\delta}$. Symbols denote experimental data, line is the model fit.

For the above mechanism, the rate of formation of N_2 and N_2O and NH_3 is $r_{N_2} = k_7 C_{N_2O} \Theta_{\text{“V”}}$, $r_{N_2O} = k_4 \Theta_{NO_{Pd}} \Theta_{\text{N“O”}} - k_7 C_{N_2O} \Theta_{\text{“V”}}$ and $r_{NH_3} = k_8 \Theta_{H_{Pd}} \Theta_{\text{N“O”}}$, respectively, $\Theta_{\text{“V”}}$ refers to fractional vacant site on the support. The rate of NO dissociation is $r_{NO} = 2r_{N_2} + 2r_{N_2O} + r_{NH_3}$. By assuming Langmuir adsorption isotherm for both H_2 and NO on the M^{n+} surface, the fraction of sites occupied by the H and NO species on the M^{n+} surface are given as $\Theta_{H_{Pd}} = \sqrt{K_1 C_{H_2}}/1 + \sqrt{K_1 C_{H_2}} + K_2 C_{NO}$ and $\Theta_{NO_{Pd}} = K_2 C_{NO}/1 + \sqrt{K_1 C_{H_2}} + K_2 C_{NO}$. By assuming equilibrium adsorption of NO on the support for step (3), $\Theta_{\text{N“O”}} = K_3 C_{NO} \Theta_{\text{“V”}}$. The steady state mass balance for the species “O” H is $\Theta_{\text{“O”H}} = k_5/k_6 \Theta_{\text{“O”}}$. Similarly the mass balance for the species “O” is

$$\Theta_{\text{“O”}} = \frac{1}{k_5\sqrt{K_1 C_{H_2}}} \left[K_2 K_3 k_4 C_{NO}^2 + k_8 K_3 C_{NO} \sqrt{K_1 C_{H_2}} + \frac{k_7 C_{N_2O}}{1 + \sqrt{K_1 C_{H_2}} + K_2 C_{NO}} \right] \Theta_{\text{“V”}}.$$

The total species balance on the support is $\Theta_{\text{“V”}} + \Theta_{\text{“O”}} + \Theta_{\text{N“O”}} + \Theta_{\text{“O”H}} = 1$ and θ_v can be obtained from this and substituted in the

expression for r_{NO}:

$$r_{NO} = \frac{2[k_7 C_{N_2O} + (K_2K_3k_4C_{NO}^2 + 0.5k_8K_3C_{NO}\sqrt{K_1C_{H_2}})/(1+\sqrt{K_1C_{H_2}} + K_2C_{NO})]}{1 + K_3C_{NO} + (k_6+k_5)/(k_6k_5\sqrt{K_1C_{H_2}})[K_2K_3k_4C_{NO}^2 + k_8K_3C_{NO}\sqrt{K_1C_{H_2}} + (k_7C_{N_2O})/(1+\sqrt{K_1C_{H_2}} + K_2C_{NO})]} \quad (D)$$

The detailed derivation is shown in S6 (see Fig. S6). The experimentally obtained rates were fitted against the calculated rate parameters with the help of nonlinear regression scheme by Levenberg–Marquardt (LM) algorithm in Polymath software. In this technique the optimized values were obtained by minimizing the sum of squared differences of the experimental rate and calculated rate. The rate parameters for the reaction with various catalysts obtained by fitting the experimental data to the model (Fig. 9b) is shown in Table 3. The rate coefficients, k_4, k_5 and k_6 are obtained from the optimization routine for $Ti_{0.9}Pd_{0.01}O_{2-\delta}$. These values were kept constant for all other catalysts. It is clear from Table 3 that as the adsorption of H_2 on M (M = Ru, Rh, Pd, Pt) (K_1) follows the trend of the molar ratio of H_2 to M in the H_2-TPR. K_2 changes in accordance with the surface area. Thus K_2 follows the order $Ti_{0.9}Ru_{0.01}O_{2-\delta} > Ti_{0.9}Rh_{0.01}O_{2-\delta} > Ti_{0.9}Pd_{0.01}O_{2-\delta} > Ti_{0.9}Pt_{0.01}O_{2-\delta}$. However, K_3 follows the order $Ti_{0.9}Pd_{0.01}O_{2-\delta} > Ti_{0.9}Pt_{0.01}O_{2-\delta}$ to $Ti_{0.9}Rh_{0.01}O_{2-\delta} > Ti_{0.9}Ru_{0.01}O_{2-\delta}$. This agrees well with our consideration of oxide ion vacancies. In $Ti_{0.9}Pd_{0.01}O_{2-\delta}$, Pd is in 2^+ state with the highest number of oxide ion vacancies, followed by $Ti_{0.9}Pt_{0.01}O_{2-\delta}$ and $Ti_{0.9}Rh_{0.01}O_{2-\delta}$ (because Pt is in mixed valent state of Pt^{2+} and Pt^{4+}, and Rh^{3+}), and $Ti_{0.9}Ru_{0.01}O_{2-\delta}$ will have the least oxide ion vacancies because Ru is in 4^+ state. Thus K_3 (NO dissociation) follows the same order as that of oxide ion vacancies. At all temperatures, the dissociation step of N_2O (k_7) is highest for $Ti_{0.9}Pd_{0.01}O_{2-\delta}$ followed by $Ti_{0.9}Pt_{0.01}O_{2-\delta}$, $Ti_{0.9}Rh_{0.01}O_{2-\delta}$ and $Ti_{0.9}Ru_{0.01}O_{2-\delta}$ (see Fig. S7), which is consistent with the selectivity of N_2O. The parameter k_8 also follows NH_3 selectivity trend obtained from the experimental findings and is zero for the Pd catalyst where no ammonia formation was observed.

3.4.2. NO reduction by H_2 in presence of excess O_2

NO reduction by H_2 in lean condition as well as NO storage and reduction are becoming popular due post combustion applications in diesel engines [38–40]. NO reduction by H_2 in lean condition over the catalyst $Ti_{0.99}Pd_{0.01}O_{2-\delta}$ was investigated with $NO:H_2:O_2 = 0.5:3:5$ (Fig. S8). Oxygen was taken in large excess. The TPR profile shows that NO conversion starts below 125 °C, reaches a maximum at 200 °C and reduces at higher temperatures. This is because at temperatures above 200 °C, H_2 is consumed by O_2 leading to formation of H_2O. The presence of O_2 enhances the N_2 selectivity (inset of Fig. S8).

3.4.3. N_2O reduction by H_2

We have shown that the reaction rate for N_2O and CO is slow as an isolated reaction but is very fast as an intermediate reaction of NO + CO [21]. This is consistent with the result of Cho [41]. $N_2O + H_2$ is also an important reaction [42] and also an intermediate in the overall $NO + H_2$ reaction [43]. It is, therefore, of interest to investigate the reaction rates of N_2O reduction with H_2 both as an isolated reaction as well as an intermediate reaction in NO and H_2. Therefore, the isolated $N_2O + H_2$ reaction was carried out over the four catalysts $Ti_{0.99}M_{0.01}O_{2-\delta}$, (M = Ru, Rh, Pd, Pt). The input gas concentration was $N_2O:H_2 = 1:3$ vol%. The light-off curve of N_2O conversion is plotted in Fig. 10a. The N_2O reduction over $Ti_{0.99}Pd_{0.01}O_{2-\delta}$ is very fast and complete conversion of N_2O occurs around 80 °C. The T_{50} of N_2O conversion over $Ti_{0.99}Pd_{0.01}O_{2-\delta}$ is only at 52 °C, whereas for $Ti_{0.99}Rh_{0.01}O_{2-\delta}$, $Ti_{0.99}Pt_{0.01}O_{2-\delta}$ and $Ti_{0.99}Ru_{0.01}O_{2-\delta}$ are at 93, 107 and 129 °C. The rate of N_2O conversion over $Ti_{0.99}Pd_{0.01}O_{2-\delta}$ for $N_2O + H_2$ reaction at 45 °C is high at 44.7×10^{-6} mol g^{-1} s^{-1}. The high rate of N_2O reduction at low temperature over $Ti_{0.99}Pd_{0.01}O_{2-\delta}$ explains the low N_2O selectivity in $NO + H_2$ reaction compared to the other catalysts.

Among all the four catalysts, $Ti_{0.99}Pd_{0.01}O_{2-\delta}$ showed the lowest temperature N_2O conversion, the kinetic modeling was done only for $Ti_{0.99}Pd_{0.01}O_{2-\delta}$ catalysts and the following reaction mechanism was proposed.

$$H_2 + 2S_{Pd} \Leftrightarrow 2H_{Pd} \quad (9)$$

$$N_2O + \text{“V”} \rightarrow N_2 + \text{“O”} \quad (10)$$

$$H_{Pd} + \text{“O”} \rightarrow \text{“O”H} + S_{Pd} \quad (11)$$

$$\text{“O”H} + H_{Pd} \rightarrow H_2O + \text{“V”} + S_{Pd} \quad (12)$$

According to this mechanism, N_2O directly dissociates on the oxide ion vacancy. Adsorbed H_2 on Pd^{2+} site reacts with oxygen in the oxide ion vacancy to produce H_2O. A rate equation can be derived using the above bi-functional mechanism. The fraction of metal surface occupied by H is $\Theta_H = \sqrt{K_9C_{H_2}}/1+\sqrt{K_9C_{H_2}}$. By assuming pseudo steady state for the species “O”, $\Theta_{\text{“O”}} = k_{10}C_{N_2O}/k_{11}(1+\sqrt{K_9C_{H_2}}/\sqrt{K_9C_{H_2}})\Theta_{\text{“V”}}$. Similarly the steady state mass balance for the species “O”H is $\Theta_{\text{“O”H}} = k_{11}/k_{12}\Theta_{\text{“O”}}$ Based on the total site balance on the support, $\Theta_{\text{“V”}} + \Theta_{\text{“O”}} + \Theta_{\text{“O”H}} = 1$ and $\Theta_{\text{“V”}} = 1/1 + k_{10}C_{N_2O}[1+\sqrt{K_9C_{H_2}}/\sqrt{K_9C_{H_2}}][1/k_{11}+1/k_{12}]$. The rate of formation of N_2 is $r_{N_2} = k_{10}C_{N_2O}\Theta_{\text{“V”}}$ and thus

$$r_{N_2} = \frac{k_{10}C_{N_2O}}{1 + k_{10}C_{N_2O}[1+\sqrt{K_9C_{H_2}}/\sqrt{K_9C_{H_2}}][1/k_{11}+1/k_{12}]} \quad (E)$$

The rate coefficients, k_{10}, k_{11}, and k_{12} are obtained from the fit of the experimental data to the model (Fig. 10b) and shown in Table 4. The rate coefficient for N_2O dissociation for the isolated reaction (k_{10}) is several orders of magnitude slower than that of the intermediate reaction (k_7), as shown in (Fig. S9).

Table 3
Rate parameters for $NO + H_2$ reaction over $Ti_{0.99}M_{0.01}O_{2-\delta}$ (M = Ru, Rh, Pd, Pt)[a]

Optimized parameters	$Ti_{0.99}Pt_{0.01}O_{2-\delta}$	$Ti_{0.99}Pd_{0.01}O_{2-\delta}$	$Ti_{0.99}Rh_{0.01}O_{2-\delta}$	$Ti_{0.99}Ru_{0.01}O_{2-\delta}$
K_1 (cm^3 mol^{-1})	6.8×10^6 $\sqrt{T}$ exp(11,600/T)	2.1×10^6 $\sqrt{T}$ exp(10,000/T)	1.6×10^6 $\sqrt{T}$ exp(9060/T)	6.9×10^5 $\sqrt{T}$ exp(8290/T)
K_2 (cm^3 mol^{-1})	8560 $\sqrt{T}$ exp(10,020/T)	10600 $\sqrt{T}$ exp(11,000/T)	10100 $\sqrt{T}$ exp(125,00/T)	10400 $\sqrt{T}$ exp(12,850/T)
K_3 (cm^3 mol^{-1})	10100 $\sqrt{T}$ exp(13,100/T)	10900 $\sqrt{T}$ exp(13,100/T)	10000 $\sqrt{T}$ exp(13,100/T)	9000 $\sqrt{T}$ exp(13,100/T)
k_7 (cm^3 g^{-1} s^{-1})	4.4×10^{17} exp(−1100/T)	1.5×10^{17} exp(−1200/T)	1.46×10^{16} exp(−1600/T)	7.58×10^{14} exp(−1900/T)
k_8 (mol g^{-1} s^{-1})	2.5×10^9 exp(−12,300/T)	0	3.4×10^7 exp(−15,100/T)	9.3×10^7 exp(−13,800/T)

[a] All other rate parameters for the four catalysts were kept constant. k_4 (mol g^{-1} s^{-1}) = 1.3×10^8 exp(−17,500/T), k_5 (mol g^{-1} s^{-1}) = 3.8 exp(−4400/T), k_6 (mol g^{-1} s^{-1}) = 4.9×10^{10} exp(−2000/T).

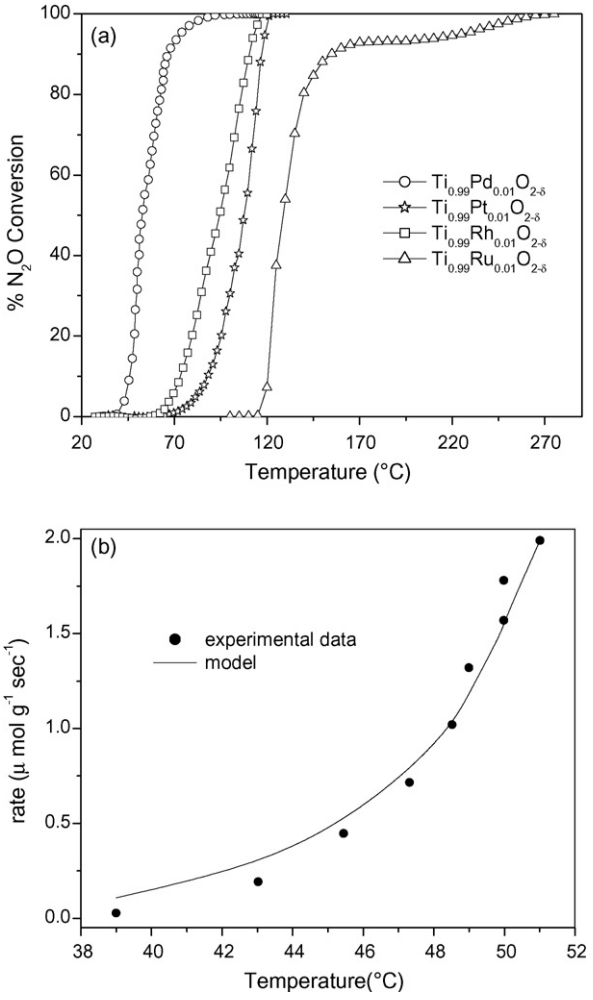

Fig. 10. (a) Light off curve of N_2O reduction by H_2 over $Ti_{0.99}M_{0.01}O_{2-\delta}$. (b) Variation of the reaction rate of $N_2O + H_2$ with temperature. Symbols denote experimental data, line is the model fit.

Table 4
Rate parameters for $N_2O + H_2$ reaction over $Ti_{0.99}Pd_{0.01}O_{2-\delta}$

Optimized parameter	$Ti_{0.99}Pd_{0.01}O_{2-\delta}$
K_9 ($cm^3\ mol^{-1}$)	$2.1 \times 10^6\ \sqrt{T}\ \exp(10{,}000/T)$
k_{10} ($cm^3\ g^{-1}\ s^{-1}$)	$8.2 \times 10^7\ \exp(-5260/T)$
k_{11} ($mol\ g^{-1}\ s^{-1}$)	$10\ \exp(-4600/T)$
k_{12} ($mol\ g^{-1}\ s^{-1}$)	$5.7 \times 10^9\ \exp(-1900/T)$

4. Conclusion

$Ti_{0.99}M_{0.01}O_{2-\delta}$ (M = Ru, Rh, Pd, Pt) synthesized by solution combustion method crystallizes in anatase phase, whereas $Ti_{0.99}Ru_{0.01}O_{2-\delta}$ only showed some impurity of rutile phase. Among all the catalysts, $Ti_{0.99}Pt_{0.01}O_{2-\delta}$ and $Ti_{0.99}Pd_{0.01}O_{2-\delta}$ show low temperature H_2 dissociation followed by $Ti_{0.99}Rh_{0.01}O_{2-\delta}$ and $Ti_{0.99}Ru_{0.01}O_{2-\delta}$. NO reduction by H_2 showed a strong correlation with the H_2-uptake study and the electrochemical study. The rate of NO reduction by H_2 follows the order: $Ti_{0.99}Pt_{0.01}O_{2-\delta} > Ti_{0.99}Pd_{0.01}O_{2-\delta} > Ti_{0.99}Rh_{0.01}O_{2-\delta} > Ti_{0.99}Ru_{0.01}$-$Ti_{0.99}Ru_{0.01}O_{2-\delta}$. $Ti_{0.99}Pd_{0.01}O_{2-\delta}$ showed the lowest N_2O and no NH_3 formation in the reaction, whereas $Ti_{0.99}Pt_{0.01}O_{2-\delta}$ showed a considerable amount of N_2O and NH_3 formation. CO poisoning effect was more prominent over $Ti_{0.99}Pt_{0.01}O_{2-\delta}$ and $Ti_{0.99}Rh_{0.01}O_{2-\delta}$, whereas it was almost negligible over $Ti_{0.99}Pd_{0.01}O_{2-\delta}$ and $Ti_{0.99}Ru_{0.01}O_{2-\delta}$. The experimental observations indicate that $Ti_{0.99}Pd_{0.01}O_{2-\delta}$ is the best catalyst among the four catalysts investigated in this study. The intermediate reaction, N_2O reduction by H_2, was also investigated and it was found that this isolated reaction was much slower than the intermediate reaction. Kinetic models were proposed for both the cases and the rate parameters were obtained by fitting the model to the experimental data.

Appendix A. Supplementary data

Supplementary data associated with this article can be found, in the online version, at doi:10.1016/j.apcatb.2008.04.008.

References

[1] A. Fritz, V. Pitchon, Appl. Catal. B 13 (1997) 1–25.
[2] H. Glick, J.J. Klien, W. Squire, J. Chem. Phys. 27 (1957) 850–857.
[3] A.M. Efstathiou, C.N. Costa, J.L.G. Fierro, U.S. Patent No. 7,105,137 B2 (2006); EP Application No. 03704721.
[4] W.C. Hecker, A.T. Bell, J. Catal. 92 (1985) 247–259.
[5] K. Tomishige, K. Asakura, Y. Iwasawa, J. Catal. 157 (1995) 472–481.
[6] Y.Z. Mergler, B.E. Nieuwenhuys, Appl. Catal. B 12 (1997) 95–110.
[7] C. Costa, A.M. Efstathiou, J. Phys. Chem. B 108 (2004) 2620–2630.
[8] K. Tanaka, A. Sasahara, J. Mol. Catal. A 155 (2000) 13–22.
[9] F.V. Caballero, L. Vicente, Chem. Eng. Sci. 58 (2003) 5087–5102.
[10] H. Hirano, T. Yamada, K.I. Tanaka, J. Siera, B.E. Nieuwenhuys, Stud. Surf. Sci. Catal. 75 (1993) 345–357.
[11] H. Hirano, T. Yamada, K.I. Tanaka, J. Siera, P. Cobden, B.E. Nieuwenhuys, Surf. Sci. 262 (1992) 97–112.
[12] S. Roy, A. Marimuthu, M.S. Hegde, G. Madras, Appl. Catal. B 71 (2007) 23–31.
[13] S.J. Tauster, S.C. Fung, R.T.K. Baker, J.A. Horsley, Science 211 (1981) 1121–1125.
[14] C.N. Costa, V.N. Stathopoulos, V.C. Belessi, A.M. Efstathiou, J. Catal. 197 (2001) 350–364.
[15] C.N. Costa, P.G. Savva, C. Andronikou, P.S. Lambrou, K. Polychronopoulou, V.C. Belessi, V.N. Stathopoulos, P.J. Pomonis, A.M. Efstathiou, J. Catal. 209 (2002) 456–471.
[16] P. Bera, M.S. Hegde, K.C. Patil, Curr. Sci. 80 (2001) 1576–1578.
[17] G. Dutta, U.V. Waghmare, T. Baidya, M.S. Hegde, Chem. Mater. 19 (2007) 6430–6436.
[18] C.N. Costa, P.G. Sawa, J.L.G. Fierro, A.M. Efstathiou, Appl. Catal. B 75 (2007) 147–156.
[19] J. Xu, R. Clayton, V. Balakotaiah, M.P. Harold, Appl. Catal. B 77 (2008) 395–408.
[20] M. Konsolakis, M. Vrontaki, G. Avgouropoulos, T. Ioannides, I.V. Yentekakis, Appl. Catal. B 68 (2006) 59–67.
[21] S. Roy, A. Marimuthu, M.S. Hegde, G. Madras, Appl. Catal. B 73 (2007) 300–310.
[22] P. Bera, K.R. Priolkar, A. Gayen, P.R. Sarode, M.S. Hegde, S. Emura, R. Kumashiro, V. Jayaram, G.N. Subbanna, Chem. Mater. 15 (2003) 2049–2060.
[23] A. Gayen, K.R. Priolkar, P.R. Sarode, V. Jayaram, M.S. Hegde, G.N. Subbanna, S. Emura, Chem. Mater. 16 (2004) 2317–2328.
[24] D.R. Penn, J. Electron. Spectrosc. Relat. Phenom. 9 (1976) 29–40.
[25] J.H. Scofield, J. Electron Spectrosc. Relat. Phenom. 8 (1976) 129–137.
[26] K. Yokota, M. Fukui, T. Tanaka, Appl. Surf. Sci. 121/122 (1997) 273–277.
[27] N. Macleod, R.M. Lambert, Catal. Commun. 3 (2002) 61–65.
[28] N. Macleod, R. Cropley, J.M. Keel, R.M. Lambert, J. Catal. 221 (2004) 20–31.
[29] N. Macleod, R.M. Lambert, Appl. Catal. B 35 (2002) 269–279.
[30] R. Burch, Catal. Today 35 (1997) 27–36.
[31] R. Burch, A.A. Shestov, J.A. Sullivan, J. Catal. 186 (1999) 353–361.
[32] A. Barrera, M. Viniegra, P. Bosch, V.H. Lara, S. Fuentes, Appl. Catal. B 34 (2001) 97–111.
[33] F. Dhainaut, S. Pietrzyk, P. Granger, Appl. Catal. B 70 (2007) 100–110.
[34] P.D. Cobden, C.A. de Wolf, M.Y. Sminov, A. Makeev, B.E. Nieuwenhuys, J Mol. Catal. A 158 (2000) 115–128.
[35] C.A. de Wolf, B.E. Nieuwenhuys, Catal. Today 70 (2001) 287–300.
[36] B. Frank, G. Emig, A. Renken, Appl. Catal. B 19 (1998) 45–67.
[37] T.E. Hoost, K. Otto, K.A. Laframboise, J. Catal 155 (1995) 303–311.
[38] M. Casapu, J.-D. Grunwaldt, M. Maciejewski, F. Krumeich, A. Baiker, M. Wittrock, S. Eckhoff, Appl. Catal. B 78 (2008) 288–300.
[39] M. Piacentini, M. Maciejewski, A. Baiker, Appl. Catal. B 72 (2007) 105–117.
[40] R.D. Clayton, M.P. Harold, V. Balakotaiah, Appl. Catal. B 81 (2008) 161–181.
[41] B.K. Cho, J. Catal. 148 (1994) 697–708.
[42] L. Xue, C. Zhang, H. He, Y. Teraoka, Appl. Catal. B 75 (2007) 167–174.
[43] A.C. Gluhoi, M.A.P. Dekkers, B.E. Nieuwenhuys, J. Catal. 219 (2003) 197–205.